Subsystem functionals in density-functional theory: Investigating the exchange energy per particle

R. Armiento*
Department of Physics, Royal Institute of Technology, Stockholm Center for Physics, Astronomy and Biotechnology, SE-106 91 Stockholm, Sweden

A. E. Mattsson†
Surface and Interface Sciences Department MS 1415, Sandia National Laboratories, Albuquerque, New Mexico 87185-1415
(Received 7 June 2002; published 31 October 2002)

A viable way of extending the successful use of density-functional theory into studies of even more complex systems than are addressed today has been suggested by Kohn and Mattsson [W. Kohn and A. E. Mattsson, Phys. Rev. Lett. **81**, 3487 (1998); A. E. Mattsson and W. Kohn, J. Chem. Phys. **115**, 3441 (2001)], and is further developed in this work. The scheme consists of dividing a system into subsystems and applying different approximations for the unknown (but general) exchange-correlation energy functional to the different subsystems. We discuss a basic requirement on approximative functionals used in this scheme; they must all adhere to a single explicit choice of the exchange-correlation energy per particle. From a numerical study of a model system with a cosine effective potential, the Mathieu gas, and one of its limiting cases, the harmonic oscillator model, we show that the conventional definition of the exchange energy per particle cannot be described by an analytical series expansion in the limit of slowly varying densities. This indicates that the conventional definition is not suitable in the context of subsystem functionals. We suggest alternative definitions and approaches to subsystem functionals for slowly varying densities and discuss the implications of our findings on the future of functional development.

DOI: 10.1103/PhysRevB.66.165117 PACS number(s): 71.15.Mb, 31.15.Ew

I. INTRODUCTION

In density-functional theory[1] (DFT) the total electron energy E_e is written as a formally exact functional of a given (arbitrary) ground-state electron density. The total electron energy for a system with an external potential $v(\mathbf{r})$ is then found as the minimum of E_e, occurring for the true ground-state electron density $n(\mathbf{r})$ of the system. The Kohn-Sham (KS) formulation[2] of DFT casts the search for this minimum into a self-consistency calculation of a problem of noninteracting electrons moving in an effective potential $v_{\text{eff}}(\mathbf{r})$. The effective potential has been constructed to make the free-electron density of the resulting free-electron orbitals, the *KS electron orbitals* $\psi_\nu(\mathbf{r})$, give the sought $n(\mathbf{r})$. In a spin unpolarized system,

$$n(\mathbf{r}) = 2\sum_{\nu} |\psi_\nu(\mathbf{r})|^2 \tag{1}$$

(where the sum is taken over all occupied orbitals).

Within KS DFT the total electron energy functional E_e is divided into classical contributions and a remaining part, the *exchange correlation energy* E_{xc}. In order to decompose E_{xc} into local contributions, the *exchange correlation energy per particle* ϵ_{xc} is defined as a density functional which gives the total exchange correlation energy as

$$E_{xc} = \int n(\mathbf{r})\epsilon_{xc}(\mathbf{r};[n])d\mathbf{r}. \tag{2}$$

This implicit definition of ϵ_{xc} is not unambiguous. All transformations preserving the value of the total integral yield possible choices of ϵ_{xc}. Equivalently expressed, two correct ϵ_{xc} are equal apart from an additive function that, multiplied with $n(\mathbf{r})$, integrates to zero over the whole system. This is an important property that we explore in this paper.

A suitable approximation of some choice of $\epsilon_{xc}(\mathbf{r};[n])$ is needed to use KS DFT in calculations. One such approximative functional put forward in the earliest works of DFT was the *local-density approximation*[2] (LDA). It was aimed at systems with very slowly varying electron densities, but was remarkably successful for wider use. LDA sets ϵ_{xc} in every space point $\mathbf{r}$, with density $n(\mathbf{r})$, equal to E_{xc} per electron of a system with a constant v_{eff} (a uniform electron gas) chosen such that the density of the uniform system equals $n(\mathbf{r})$. In this way LDA uses as input only the local value of the density and can be written as $\epsilon_{xc}^{\text{LDA}}(n(\mathbf{r}))$. Newer functionals, *generalized gradient approximations* (GGA's), use, apart from the local value of the density, also the first-order density derivative (the gradient): $\epsilon_{xc}^{\text{GGA}}(n(\mathbf{r}),|\nabla n(\mathbf{r})|)$. Further functional development such as meta-GGA's, use additional parameters not always trivially related to the density, e.g., kinetic energy densities.

The successively refined approximations of $\epsilon_{xc}(\mathbf{r};[n])$ described above all take the slowly varying density as their starting points. The aim has been to create a single universal functional useful for all kinds of systems, but the resulting functionals tend to fail in the parts of the system where the density is far from homogeneous, e.g., at surfaces.[3–5] In contrast to this practice of developing universal functionals, Kohn and Mattsson[6] (KM) worked towards a functional specifically designed to handle the edge part of a system. They suggested that this functional could be used together with another functional taking care of the interior region of the system. A more generalized idea of using different functionals in different regions of a system is illustrated in Fig. 1.

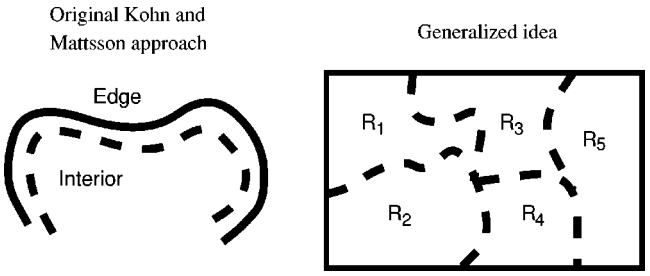

FIG. 1. The generalized idea of dividing a system into subsystems, applying different functionals to the different parts. The left figure refers to the approach presented by Kohn and Mattsson in Ref. 6.

Functionals used in this way must all adhere to a single explicit choice of the exchange-correlation energy per particle. This is an important requirement that is discussed in this paper.

KM introduced the *edge electron gas* as a suitable starting point for a functional to use in the edgelike part of a system. The simplest possible model of the edge electron gas, the *Airy gas*, has a linear effective potential and features wave functions transitioning from oscillatory to vanishing. A functional based on the Airy gas does not relate the density in the edge subsystem to a slowly varying density, but is instead based on other assumptions valid only in an appropriate region near an edge. Within this region of validity an Airy gas based functional should outperform functionals based on the homogeneous electron gas, but may not be a suitable approximation in the bulk part or interior of a system.

In a related effort Vitos *et al.* have developed a functional, the *local Airy gas* (LAG).[7] Roughly, it corresponds to using the Airy gas exchange energy per particle and the LDA correlation energy per particle in the edge region, while using LDA exchange and correlation energies per particle in the interior region. LAG gives mixed results for two reasons. First, the LDA correlation functional used in the edge region is not compatible[8] with the Airy gas exchange functional. Second, the use of LDA in the interior region is, in many cases, inadequate. An Airy gas based correlation functional and an improved interior region functional are needed to improve on the LAG.

The uniform electron gas and the edge electron gas are not the only interesting starting points for functionals. Other alternatives should be used to develop functionals for a large variety of subsystem classes. Such functionals can either be carefully combined by computational scientists targeting some specific system, or be composed into more general functionals applicable to a general set of problems, such as systems with electronic edges, which was the aim of the original work of KM.[6] Functionals derived from alternative starting points have already been created, for example for Luttinger liquid systems.[9]

In addition to the general discussions about the use of functionals in subsystems, this work also addresses the development of a functional suitable for the interior region of a system, where the density is slowly varying. We determine if a specific (the conventional) choice of the exchange energy per particle can be expressed as a power expansion in the density variation. The investigation is based on the Mathieu gas (MG) model, a noninteracting electron system that models the KS orbitals of an effective potential with a cosine in one of the three dimensions. The MG is presented in detail, as its properties are important for the interpretation and discussion of our results. It shows a rudimentary energy-band structure and its parameter space range from the free-electron (FE) gas to a harmonic oscillator (HO) system. From numerical calculations of the MG we show that the conventional choice of the exchange energy per particle has a nonanalytical behavior in the limit of slowly varying densities, and thus this choice cannot be described by an ordinary (analytical) expansion. The behavior indicates that the conventional definition of the exchange energy per particle is not a good choice for the derivation of subsystem functionals. Our results also raise concerns for the inclusion of Laplacian terms in functionals outside the scheme of subsystem functionals. The discovered nonanalyticity is argued from extensive numerical data for the MG. This presented data might also be useful outside of our present work for derivation and testing of exchange functionals.

In Sec. II, we explain and explore the basic requirement that suitable subsystem functionals in a divided system scheme must all adhere to a single explicit choice of the exchange-correlation energy per particle. This is explicitly discussed in the context of the exchange energy per particle in a slowly varying system. In Sec. III, the MG is thoroughly presented and its HO limit is recognized as a valuable model system in its own right. In Sec. IV the computed density, density Laplacian, and exchange energy per particle are analyzed in terms of deviations from their uniform electron gas values, and finite-size oscillations present in the HO-like part of the MG parameter space are investigated. The deviations from the uniform gas values for the density and the Laplacian are shown to behave as expected, but the computed deviations from the uniform electron gas value for the exchange energy per particle imply that the conventional definition of the exchange energy per particle must be modeled by an nonanalytical function of the Laplacian. In Sec. V the numerical precision of our data is validated. Finally, in Sec. VI, our findings are summarized and discussed, with comments on the future development of subsystem functionals.

II. EXCHANGE ENERGIES PER PARTICLE

The basic idea explored in this work is to divide the integration over the whole system in Eq. (2) into suitable parts and apply different approximations of the exchange-correlation energy per particle, $\epsilon_{xc}(\mathbf{r},[n])$ to each part. Approximations of $\epsilon_{xc}(\mathbf{r},[n])$, which can be applied to such a divided system, are referred to as *subsystem functionals*. In this section we will discuss requirements a subsystem functional must satisfy.

At this point we are only concerned with the exchange contribution to the exchange-correlation energy per particle. The exchange and correlation terms are separated in the usual way

$$\epsilon_{xc} = \epsilon_x + \epsilon_c . \tag{3}$$

The freedom of choice of ϵ_{xc}, as explained in connection to Eq. (2), also makes ϵ_x nonunique. Similarly as for ϵ_{xc}, all choices of ϵ_x must integrate, multiplied with the electron density, to the same value (the total exchange energy E_x; Ref. 10 presents several definitions of E_x and discusses how they relate to different choices of ϵ_x). Let $\epsilon_x^{\mathrm{irxh}}$ be the conventional choice of ϵ_x, which was also used for the Airy gas.[6] There exists an exact relation[11] between this exchange energy per particle and the KS orbitals. Using the *first-order spinless density matrix* $\rho_1(\mathbf{r};\mathbf{r}')$ and the *inverse radius of the exchange hole*[6] (irxh), R_x^{-1}, the relation is expressed in cgs units as

$$\epsilon_x^{\mathrm{irxh}} = -e^2 R_x^{-1}(\mathbf{r})/2, \tag{4}$$

$$R_x^{-1}(\mathbf{r}) = -\int \frac{n_x(\mathbf{r};\mathbf{r}')}{|\mathbf{r}-\mathbf{r}'|} d\mathbf{r}', \tag{5}$$

$$n_x(\mathbf{r};\mathbf{r}') = -\frac{1}{2}\frac{|\rho_1(\mathbf{r};\mathbf{r}')|^2}{n(\mathbf{r})}, \tag{6}$$

$$\rho_1(\mathbf{r};\mathbf{r}') = 2\sum_\nu \psi_\nu(\mathbf{r})\psi_\nu^*(\mathbf{r}'), \tag{7}$$

where $n_x(\mathbf{r};\mathbf{r}')$ is the conventional exchange hole density and e is the electronic charge.

A. Systems with slowly varying densities

For slowly varying densities, the exchange part of LDA is the most straightforward approximation of $\epsilon_x^{\mathrm{irxh}}(\mathbf{r};[n])$. The LDA expression is obtained by inserting KS orbitals for a constant effective potential (plane waves) in Eqs. (4)–(7), giving a constant $\epsilon_x^{\mathrm{irxh}}$, which is parametrized in the uniform electron density to give the familiar expression

$$\epsilon_x^{\mathrm{LDA}}(n(\mathbf{r})) = -e^2\frac{3}{4\pi}[3\pi^2 n(\mathbf{r})]^{1/3}. \tag{8}$$

An improvement to LDA exchange, proposed in the earliest works on DFT,[2] was to use gradient expansions. The traditional gradient approximation approach results in the *second-order gradient expansion approximation* (GEA),

$$\epsilon_x^{\mathrm{GEA}}(n(\mathbf{r}),|\nabla n(\mathbf{r})|) = \epsilon_x^{\mathrm{LDA}}(n(\mathbf{r}))\left(1+\frac{10}{81}s^2\right), \tag{9}$$

where s is the *dimensionless gradient*,

$$s = \frac{|\nabla n(\mathbf{r})|}{2(3\pi^2)^{1/3} n^{4/3}(\mathbf{r})}. \tag{10}$$

The correct coefficient, 10/81, of the dimensionless gradient s was finally established by Kleinman and Lee[12] in 1988. In a truly slowly varying system, the GEA performs well, but outside of its area of formal validity the GEA is found to be unsatisfactory when applied in computations. Often it is less accurate than the LDA.[13] However, GEA has successfully been used in the derivation of modern nonempirical GGAs as the limit of low-density variation, and has led to very useful functionals.[14,15]

In addition to the dimensionless gradient term, there is another term that should be included in a general expansion. This term is proportional to the *dimensionless Laplacian*,

$$q = \frac{\nabla^2 n(\mathbf{r})}{4(3\pi^2)^{2/3} n^{5/3}(\mathbf{r})}. \tag{11}$$

In the following it is explained why this term can be neglected in GEA and why it is not appropriate to neglect it in the present context of different functionals in different parts of a system.

By Green's formula

$$\int_V n^{4/3}\left(\frac{\nabla^2 n}{n^{5/3}} - \frac{1}{3}\frac{|\nabla n|^2}{n^{8/3}}\right) dV - \oint_S n^{-1/3}\frac{\partial n}{\partial \xi} dS = 0, \tag{12}$$

where $\partial n/\partial \xi$ is the derivative of the density in the direction of the outward pointing normal to the surface S enclosing the volume V. Equation (12), showing one choice of a function integrating to zero, can be added to the exchange part of Eq. (2). Adding the integrand of Eq. (12), multiplied by a factor proportional to b, to the GEA, Eq. (9), the expansion of all possible analytical exchange energies per particle becomes

$$\epsilon_x(\mathbf{r};[n]) = \epsilon_x^{\mathrm{LDA}}(n(\mathbf{r}))\left[1+\left(\frac{10}{81}-\frac{b}{3}\right)s^2 + bq + \cdots\right], \tag{13}$$

where the surface term always vanishes in practical calculations. In a finite system the integration surface is placed far outside the system, where the normal derivative of the density is very small. Furthermore, the integrands at opposite sides of the surface cancel due to the opposite sign of the directional derivatives of the density. In a periodic system the integrands on opposite sides of the cell also cancel, since their normals are in opposite directions. Finally, in a divided system, any surface element on the surfaces enclosing the different parts of the system have another surface element with opposite sign that can cancel *if the constant b is the same for the different functionals used*. Hence, as long as the same functional is used in the whole system, the value of b can be arbitrary. It is traditionally set to zero, motivating that GGAs need only depend on the gradient and not on the Laplacian. In a divided system, however, all subsystem functionals used must have the same value of b. Unfortunately, an explicit definition of the exchange energy per particle resulting in $b=0$ is not known. In the choice between searching for such a definition or establishing the value of b that corresponds to the definition in Eqs. (4)–(7) we here choose the latter.

Turning to our choice of exchange energy per particle, the expansion takes the form

$$\epsilon_x^{\mathrm{irxh}}(\mathbf{r};[n]) = \epsilon_x^{\mathrm{LDA}}(n(\mathbf{r}))(1 + a^{\mathrm{irxh}}s^2 + b^{\mathrm{irxh}}q + \cdots), \tag{14}$$

where the gradient coefficient a^{irxh} is expected to be $10/81 - b^{\mathrm{irxh}}/3$, and the Laplacian coefficient b^{irxh} is to be determined. Since the gradient coefficient is fully determined by the Laplacian coefficient we will only be concerned with the Laplacian coefficient.

B. General systems

Although only slowly varying systems are explicitly examined in this work, we comment on the extension of subsystem functionals to general systems. Above we discussed the requirement that all subsystem exchange functionals applied to one slowly varying system must have the same value of the Laplacian coefficient b. The same arguments can be repeated for all terms in the Taylor expansion, leading to the conclusion that different subsystem exchange functionals applied to a general system must all be based on the same explicit definition of the exchange energy per particle. This point was illustrated by assuming the exchange energy per particle to be analytic. However, it is obvious that analyticity is not required. Hence, to be a subsystem functional, a full exchange-correlation functional must be based on a specific set of definitions. When the integration in Eq. (2) is divided into integrations over subsystems, new nonvanishing terms must not be introduced.

III. MATHIEU GAS

The development of exchange-correlation energy functionals has predominately been guided by studies of one model system, the uniform electron gas. For example, the Monte Carlo calculation by Ceperly and Alder[16] of the total energy of uniform gases with different densities is the foundation of most correlation functionals in use today, and the exchange energy of the uniform electron gas is the basis for the LDA exchange energy functional.[2] Other model systems, like the Airy gas[6] and the exponential model,[17] have been studied to expand the understanding of strongly inhomogeneous systems such as surfaces. Sahni and co-workers used model systems, like the step, linear, and finite-linear potential models, in studies of surfaces.[18]

One motivation for using model systems is the unified development of exchange and correlation functionals. LDA performs so well since the LDA exchange and correlation functionals are ''compatible.''[8] The error in the LDA exchange is counterbalanced by the error in the LDA correlation, as the combination gives the energy in the uniform electron gas. This is in contrast to how GGA's are usually developed, where the exchange and correlation functionals are constructed separately, as accurately as possible, and little attention is paid to the combined quantity. It is well known that even though the separate GGA exchange and correlation energies for the jellium surface are much more accurate that the LDA quantities, the combined quantity is actually more accurate in LDA than in GGA (Ref. 19) [this is, however, not true[20] for the PKZB meta-GGA (Ref. 21)]. By creating functionals from model systems it is possible to obtain compatible exchange and correlation.

Our aim is to go beyond LDA, basing our study on a model system suitable for interior regions, containing the slowly varying limit where LDA is appropriate. We seek information about the exchange functional from exploration of yet another model system, the Mathieu Gas (MG). The MG is the two-parameter model in which the KS effective potential is described by (Fig. 2)

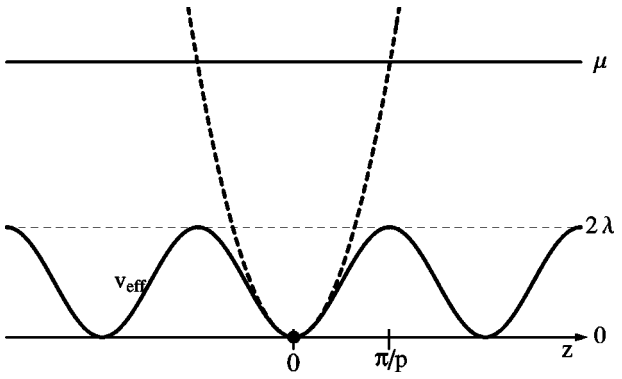

FIG. 2. The effective potential of the Mathieu Gas (MG). The dot marks a minimum point, i.e., one of the points where the dimensionless gradient vanishes. For amplitudes 2λ much larger than the chemical potential μ, the MG approaches the harmonic oscillator (HO) model, whose effective potential is shown as a fat broken line. The opposite limit is the free-electron (FE) gas. The limiting case between the HO domain and the FE domain arises when $2\lambda = \mu$.

$$v_{\mathrm{eff}}(z) = \lambda - \lambda \cos(pz). \tag{15}$$

where λ is the amplitude, and p is the wave vector of the effective potential. Since we are mainly interested in the Laplacian coefficient b^{irxh} in Eq. (14), we have chosen $z=0$ to be at a local minimum in the symmetric effective potential. The dimensionless gradient in Eq. (10) is always zero at this point, thus eliminating the gradient term.

The dimensionless parameters of this family of potentials are $\bar{\lambda} = \lambda/\mu$ and $\bar{p} = p/(2k_{F,u})$, where $k_{F,u}^2 = 2m\mu/\hbar^2$ is the Fermi wave vector of a uniform electron gas *with chemical potential* μ. In this work $k_{F,u}$ is considered to be independent of position.

A system similar to the MG has recently been studied by Nekovee *et al.*[22] using Monte Carlo methods, but with emphasis on strongly inhomogeneous densities. As early as 1952 Slater studied a potential with cosines in all three directions.[23] Some of his results are relevant in our context and will be repeated here.

A. Exact solution of the MG

Following the general method outlined in Ref. 6,

$$\psi_\nu(x,y,z) = \frac{1}{A^{1/2}} e^{i(k_1 x + k_2 y)} \varphi_\eta(z) \tag{16}$$

is inserted into the KS equations[2] [$\nu \equiv (k_1, k_2, \eta)$; $k_i L_i = 2\pi m_i$ ($i=1,2$, m_i integer), and $A \equiv L_1 L_2$ the cross-sectional area]. The solutions to the resulting equation for $\varphi_\eta(z)$,

$$\left(-\frac{\hbar^2}{2m}\frac{d^2}{dz^2} + v_{\text{eff}}(z) - \epsilon_\eta \right) \varphi_\eta(z) = 0, \tag{17}$$

with $v_{\text{eff}}(z)$ from Eq. (15), can be written in terms of Mathieu functions, $F_\eta(x)$. These functions are described in Ref. 24. We use the Bloch, or Floquet, form:

$$\varphi_\eta(z) = \frac{1}{\sqrt{L_3}} F_\eta(\overline{pz}) = \frac{1}{\sqrt{L_3}} \exp(i\,\eta\overline{pz}) \sum_{k=-\infty}^{\infty} c_{2k}^\eta \exp(i2k\overline{pz}), \tag{18}$$

where $\eta\overline{p}k_{F,u}L_3 = 2\pi m_3$ (m_3 integer), L_3 the z length of the system, $\overline{z} = k_{F,u}z$, and the parameter η is the characteristic exponent. The coefficients c_{2k}^η are determined from

$$(2k+\eta)^2 c_{2k}^\eta - \frac{\overline{\lambda}}{2\overline{p^2}}(c_{2k-2}^\eta + c_{2k+2}^\eta) = a\left(\eta, \frac{\overline{\lambda}}{2\overline{p^2}}\right) c_{2k}^\eta, \tag{19}$$

and are normalized with $\Sigma_{k=-\infty}^{\infty} |c_{2k}^\eta|^2 = 1$. These equations also give the eigenvalues $a(\eta, \overline{\lambda}/(2\overline{p^2}))$ used in the energy. The energy of an eigenstate of the MG is

$$\epsilon_\nu = \frac{\hbar^2}{2m}(k_1^2 + k_2^2) + \epsilon_\eta \leqslant \mu, \tag{20}$$

where

$$\frac{\epsilon_\eta}{\mu} = \overline{\lambda} + \overline{p}^2 a\left(\eta, \frac{\overline{\lambda}}{2\overline{p^2}}\right). \tag{21}$$

Equation (19) can be written in an infinite symmetric matrix form. Matrix theory gives that all values of $a(\eta, \overline{\lambda}/(2\overline{p^2}))$ are real and bounded from below. The same system of equations is recovered while shifting η by an even integer. The values $a(\eta, \overline{\lambda}/(2\overline{p^2}))$ also has a $\pm\eta$ symmetry. The index η have infinite range, $-\infty < \eta < \infty$, and with each value one energy and one wave function are associated. This is the extended Brillouin-zone scheme. An alternative is to set $\eta =$ even integer $+\zeta$, $-1 < \zeta \leqslant 1$, and associate an infinite number of different wave functions and energies with each value of ζ. This is the reduced Brillouin-zone scheme. Note, in the extended scheme, that $\eta =$ integer will seemingly produce two solutions as the $\pm\eta$ symmetry coincides with the even-integer shift symmetry. The issue is resolved by noting that one of the solutions is associated with the $\eta = -|\text{integer}|$ and the other with $\eta = |\text{integer}|$. This is further discussed in association with the energy-band structure of the MG.

Both the Mathieu functions (in their real forms, see Appendix B) and $a(\eta, Q)$ are available in numerical computer software (e.g., MATHEMATICA), making it easy to reproduce most of Slaters results.[23]

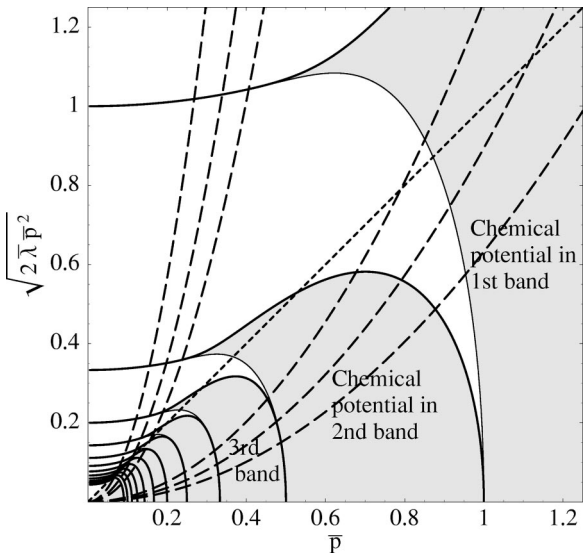

FIG. 3. The parameter space of the MG. Parameters in the shaded areas correspond to a chemical potential in one of the bands, while parameters in the light areas correspond to a chemical potential in the free-electron continuum between bands. For combinations of parameters on the full lines the chemical potential is at a band edge. Thick lines correspond to the bottom of bands, while thin lines correspond to the top of bands. For the sake of clarity lines near the origin are not shown. The short-dashed line is the dividing line between the HO domain and the FE domain (see text) and corresponds to a chemical potential at the maximum of the effective potential (Fig. 2). For combinations of parameters on a quadratic line the energy-band structure is constant (see Fig. 4 and text) apart from scaling. From right to left the long-dashed quadratic lines correspond to $\overline{\lambda}/\overline{p^2} = 0.2$, 0.4, 0.8, 20, 40, and 100.

B. Parameter space

The parameter space of the MG contains two well studied limiting cases; the weakly perturbed periodic potential [the free-electron (FE) gas] and the harmonic oscillator (HO). The two dimensionless parameters of the MG are $\overline{\lambda}$ and $\overline{p}$, but in discussions of certain properties there are dimensionless combinations that work better, most notably the combinations $\sqrt{2\overline{\lambda}\overline{p^2}}$, in the HO limit, and $\overline{\lambda}/\overline{p^2}$, when discussing the energy-band structure. In order to emphasize the two dimensionality of the parameter space we do not introduce new notations for these combinations. In the next sections the different combinations and their meaning are discussed. We have chosen to use a parameter space spanned by $\overline{p}$ and $\sqrt{2\overline{\lambda}\overline{p^2}}$ as is shown in Fig. 3.

1. Periodic potential and $\overline{p}$

The parameter $\overline{p}$ describes the periodicity of the potential. The vector $2\overline{p}k_{F,u}\hat{z}$ (where $\hat{z}$ is a unit vector in the z direction) is the reciprocal-lattice vector. All k-space vectors, $(k_1, k_2, \eta\overline{p}k_{F,u})$, with a magnitude of the z component being a multiple of $\overline{p}k_{F,u}$ (i.e., with integer η) lie on Bragg planes. For a detailed discussion of the weak periodic potential see

Ref. 25. In the parameter space shown in Fig. 3, lines with constant $\bar{p}$ are parallel to the vertical axis.

2. FE gas limit and $\bar{\lambda}$

As $\bar{\lambda}\to 0$, the system of equations in Eq. (19) decouples and

$$\varphi_\eta(z)=\frac{1}{\sqrt{L_3}}\exp(i\eta\bar{p}z), \tag{22}$$

$$\frac{\epsilon_\eta}{\mu}=\eta^2\bar{p}^2. \tag{23}$$

By substituting $k_3=\eta\bar{p}k_{F,u}$, the plane waves of the uniform electron gas are recognized.

Lines with constant $\bar{\lambda}$ are straight and start at the origin, like the short-dashed line $\bar{\lambda}=1/2$, in the parameter space shown in Fig 3. The horizontal axis, $\bar{\lambda}=0$, is the FE gas (or uniform electron gas) limit.

3. HO and $\sqrt{2\bar{\lambda}\bar{p}^2}$

For $\bar{\lambda}=\lambda/\mu\to\infty$ (see dashed line in Fig. 2) the occupied energy levels are well described by a harmonic oscillator. The cosine potential can be expanded around $z=0$ to lowest order,

$$v_{\text{eff}}(z)=\frac{\lambda p^2}{2}z^2, \tag{24}$$

giving the HO model.

The discrete energy levels in the z direction in k space of this system are proportional to $\sqrt{2\bar{\lambda}\bar{p}^2}$,

$$\frac{\epsilon_n}{\mu}=\sqrt{2\bar{\lambda}\bar{p}^2}(2n+1). \tag{25}$$

The KS orbitals are

$$\varphi_n(z)=\left(\frac{k_{F,u}(\sqrt{2\bar{\lambda}\bar{p}^2})^{1/2}}{\sqrt{\pi}2^n n!}\right)^{1/2}H_n((\sqrt{2\bar{\lambda}\bar{p}^2})^{1/2}\bar{z})\times\exp(-[(\sqrt{2\bar{\lambda}\bar{p}^2})^{1/2}\bar{z}]^2/2), \tag{26}$$

where $H_n(x)$ are Hermite polynomials[24] and $n=0, 1, 2, \ldots$. The vertical axis in the parameter space in Fig. 3 is the HO limit and lines with constant $\sqrt{2\bar{\lambda}\bar{p}^2}$ are parallel to the horizontal axis.

4. Curvature and $\bar{\lambda}\bar{p}^2$

The dimensionless Laplacian q in Eq. (11) of the minimum (black dot in Fig. 2) is, to first order, proportional to the curvature there. The (dimensionless) curvature is proportional to $\bar{\lambda}\bar{p}^2$, as is seen from Eq. (24).

C. Energy-band structure and $\bar{\lambda}/\bar{p}^2$

Due to the uniform character of the effective potential in the x and y directions, the MG has a continuous energy spectrum. [Only the case where the linear dimensions, L_i $(i=1,2,$ and $3)$, of the system are infinite, i.e., k space is dense, is considered.] The density of states at the chemical potential only depends on the energy-band structure in the z direction in k space, that is, on the structure of ϵ_η, since for any $\epsilon_\eta\leqslant\mu$, there is always a free-electron energy addition that brings the total energy to the chemical potential according to Eq. (20). However, the MG does exhibit a rudimentary band structure due to the Bragg planes in the z direction of k space. The characteristic exponent η plays the role of a dimensionless scaled wave vector. Energies in the first band are given by $0<|\eta|<1$, energies in the second band by $1<|\eta|<2$, and so on. Note, however, that there are never any band gaps. The chemical potential can be placed in the free-electron continuum between two bands. In Sec. IV it is shown that this band structure influences the quantities calculated for the MG.

Recall that $k_{F,u}$ is not the magnitude of the Fermi wave vector of a MG system with chemical potential μ, but that of the Fermi wave vector of a uniform electron gas with chemical potential μ. The Fermi surface for the general MG system is determined by the k vectors fulfilling $\epsilon_\nu=\mu$ in Eq. (20).

The energy in Eq. (21) can be scaled in two ways, each appropriate for one of the limiting cases:

$$\frac{1}{\bar{p}^2}\frac{\epsilon_\eta}{\mu}=\frac{\bar{\lambda}}{\bar{p}^2}+a\left(\eta,\frac{\bar{\lambda}}{2\bar{p}^2}\right)\xrightarrow{\bar{\lambda}/\bar{p}^2\to 0}\eta^2 \tag{27}$$

and

$$\frac{1}{\sqrt{2\bar{\lambda}\bar{p}^2}}\frac{\epsilon_\eta}{\mu}=\left(\frac{\bar{\lambda}}{2\bar{p}^2}\right)^{1/2}+\left(\frac{\bar{p}^2}{2\bar{\lambda}}\right)^{1/2}a\left(\eta,\frac{\bar{\lambda}}{2\bar{p}^2}\right)\xrightarrow{\bar{\lambda}/\bar{p}^2\to\infty}(2n+1), \tag{28}$$

where n is the integer nearest below $|\eta|$.

The FE gas limit is obtained when $\bar{\lambda}/\bar{p}^2\to 0$. For FE like spectra, scaling according to Eq. (27) is appropriate. The HO limit is when $\bar{\lambda}/\bar{p}^2\to\infty$ and, for HO-like spectra, scaling according to Eq. (28) is used. In Fig. 4 we show four scaled energy-band structures.

Apart from scaling, the energy spectra are the same for parameters related by constant $\bar{\lambda}/\bar{p}^2$ [see Eqs. (27) and (28)]. In Fig. 3 (the parameter space spanned by $\bar{p}$ and $\sqrt{2\bar{\lambda}\bar{p}^2}$), long-dashed lines represent $\bar{\lambda}/\bar{p}^2=0.2$, 0.4, 0.8, 20, 40, and 100. The x axis corresponds to the FE gas limit, $\bar{\lambda}/\bar{p}^2=0$, and the y axis represents the HO model, $\bar{\lambda}/\bar{p}^2\to\infty$. Note that $\bar{\lambda}/\bar{p}^2$ is independent of the chemical potential μ. Fixing the chemical potential in the energy-band structure selects a specific point on a line with constant $\bar{\lambda}/\bar{p}^2$, and thereby sets the scale of the energy-band structure.

In Fig. 3 the full lines show choices of parameters for which the chemical potential is placed on an energy level/on

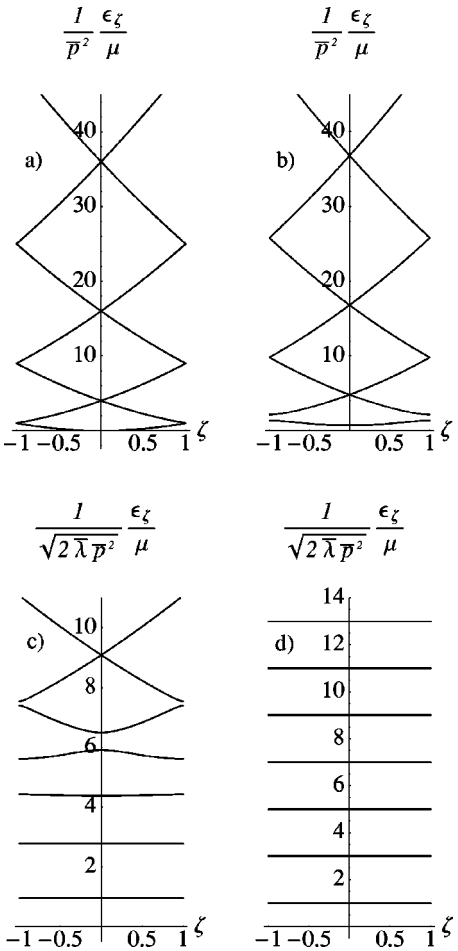

FIG. 4. The energy band structure of selected MG models: (a) $\bar{\lambda}/\bar{p^2}=0$, the FE limit, (b) $\bar{\lambda}/\bar{p^2}=0.8$, (c) $\bar{\lambda}/\bar{p^2}=20$, and (d) $\bar{\lambda}/\bar{p^2}\rightarrow\infty$, the HO limit. The reduced index $\zeta(-1<\zeta\leqslant 1)$ is related to $\eta(-\infty<\eta<\infty)$ by $\eta=$even integer$+\zeta$.

a band edge. The energy levels of the HO broaden into energy bands as the potential becomes weaker and thereby allows for tunneling between neighboring wells. The short-dashed line with $\bar{\lambda}=1/2$ marks where the chemical potential is equal to the maximum of the effective potential (see Fig. 2). This line separates HO-like and FE-like systems.

Within a fixed energy structure (where $\bar{\lambda}/\bar{p^2}$ is constant) a FE-like state is always reached when the chemical potential is raised well above the effective potential (i.e., going towards the origin on a line with a constant $\bar{\lambda}/\bar{p^2}$ and passing the short-dashed $\bar{\lambda}=1/2$ line). This is seen in Fig. 4(c).

The slowly varying limit is at the origin. In this work paths with constant $\bar{\lambda}/\bar{p^2}$ are followed towards the origin, but any path towards the origin is equally valid.

The position of the chemical potential relative to the different energy levels ϵ_η is important, and a parameter for this property is needed. We choose the definition

$$\alpha=\frac{\mu-\epsilon_{\eta_1}}{\epsilon_{\eta_2}-\epsilon_{\eta_1}}+|\eta_1|, \tag{29}$$

where, if μ is inside a z-dimension energy band, ϵ_{η_1} is the lowest energy in this band. If μ is not inside an energy band, ϵ_{η_1} is the lowest energy in the band which contains the z-dimension energy state with highest energy $\leqslant\mu$. Furthermore, ϵ_{η_2} is the lowest possible energy of all z-dimension energy states within bands that only contain energies $>\mu$. By construction η_1 and η_2 are integer.

The parameter α describes the position of the chemical potential relative to the lower band edges, that is, the lowest energies of the energy bands in the z dimensional energy band structure. The parameter α differs from η in that it indexes values of the chemical potential both within and between the energy bands in the z dimension, making it useful throughout the parameter space of the MG. Integer α (lower band edges) are shown as thick lines in Fig. 3.

In the pure HO model $|\eta_1|$ approaches the index of the highest discrete energy level with energy $\leqslant\mu$. Thus it is easy to retrieve the (integer) value of this highest index by truncating the α parameter. Furthermore, for the HO model and the FE limit it is straightforward to express the α parameter in $\bar{\lambda}$ and $\bar{p}$ (where $\lfloor x\rfloor$ is the highest integer $\leqslant x$):

$$\alpha_{HO}=\frac{1}{2\sqrt{2\bar{\lambda}\bar{p^2}}}-\frac{1}{2}, \tag{30}$$

$$\alpha_{FE}=\frac{1/\bar{p^2}+N(N+1)}{2N+1},\quad N=\left\lfloor\frac{1}{\bar{p}}\right\rfloor. \tag{31}$$

A similar explicit expression can not be constructed for the general MG case. After inserting Eq. (21) in Eq. (29) the expression cannot be further simplified. In addition, when using Eq. (21) for energies of band edges (i.e., integer η, as is the case here) extra care must be taken not to confuse the lowest energy in a band with the highest energy in the band below, corresponding to the two different signs of the integer η. For noninteger η both signs give identical energies.

IV. DENSITY, DENSITY LAPLACIAN AND IRXH EXCHANGE ENERGY PER PARTICLE IN THE MG

In this section we will use the framework of the MG developed above to examine a number of DFT quantities. The primary purpose of this study is to investigate the proposed exchange energy per particle expansion of Eq. (14). The presentation will be kept on a detailed part by part level, which is needed to show the true origin of the odd behavior that is found. A higher level summary and discussion of the results is deferred to Sec. VI.

Infinite systems are considered; $L_1,L_2,L_3\rightarrow\infty$, and the k vectors, k_1,k_2, and η, are continuous variables. The FE limit is solved by inserting the plane wave KS orbitals, Eq. (22) and Eq. (16), into the definition of the density, Eq. (1), and the definition of the exchange energy per particle, Eqs. (4)–(7). The well known results are

$$n_u(\mathbf{r})=\frac{k_{F,u}^3}{3\pi^2}, \tag{32}$$

$$\epsilon_{x,u}^{\mathrm{irxh}}(\mathbf{r}) = -e^2 \frac{3k_{F,u}}{4\pi}. \tag{33}$$

Using Eqs. (1) and (4)–(7) we calculate the densities $n_m(\mathbf{r})$ and $n_h(\mathbf{r})$ and the exchange energies per particle $\epsilon_{x,m}^{\mathrm{irxh}}(\mathbf{r})$ and $\epsilon_{x,h}^{\mathrm{irxh}}(\mathbf{r})$ for the MG and the HO, respectively. From the calculated densities, density Laplacians and gradients are obtained numerically. Details on numerical methods and calculational schemes are presented in the appendixes.

A. Analyzing the results: Expanding around the uniform electron gas

For clarity parameters directly related to the MG are used in the analysis and, unless otherwise stated, the $z=0$ point is considered. Instead of relating the calculated exchange energy per particle, $\epsilon_x^{\mathrm{irxh}}$, to the LDA values as in Eq. (14) (i.e., relate it to the exchange energy of a uniform electron gas with the same density), it is related to the exchange energy of a uniform electron gas with the same chemical potential.

With a curvature on the potential not only the exchange energy per particle but also the density and the Laplacian deviate from the uniform electron gas values. To lowest order

$$n_m(0) = n_u(1 + a_1\overline{\lambda p^2}), \tag{34}$$

$$q_m(0) = a_2\overline{\lambda p^2}, \tag{35}$$

$$\epsilon_{x,m}^{\mathrm{irxh}}(0) = \epsilon_{x,u}^{\mathrm{irxh}}(1 + a_3\overline{\lambda p^2}), \tag{36}$$

where n_u and $\epsilon_{x,u}^{\mathrm{irxh}}$ are given in Eqs. (32) and (33). From Eq. (8) it then follows that

$$b^{\mathrm{irxh}} = \frac{a_3 - a_1/3}{a_2}. \tag{37}$$

The prefactors $a_1, a_2,$ and a_3 remain to be determined.

B. Determination of the coefficient of density deviation, a_1

We first examine the quantity

$$\frac{[n_m(0)/n_u - 1]}{\overline{\lambda p^2}} \xrightarrow{\overline{\lambda p^2}\to 0} a_1. \tag{38}$$

Figure 5 shows this density deviation of the MG, at the minimum point, from a uniform electron gas with the same chemical potential scaled with the curvature. In Fig. 6 the same data are shown as a contour plot with the energy-band structure in Fig. 3 superimposed. A dependence of the density deviation on the energy-band structure is evident.

A dramatic change happens in the behavior along the line where the chemical potential is at the potential maximum, $\overline{\lambda} = 1/2$, that is, at the line dividing the HO-like and the FE-like domains. This change occurs where the chemical potential rises above the most distinct discrete energy level and enters a more continuous energy-band structure, once again illustrating the importance of the energy-band structure for the properties of the system.

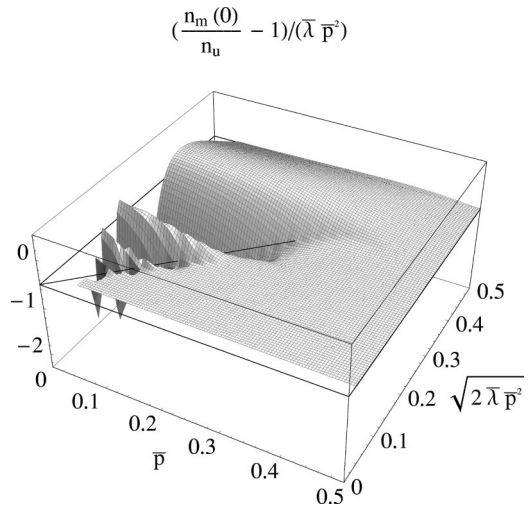

FIG. 5. The density deviations in the minimum point of the MG (cf. Fig. 2), $[n_m(0)/n_u - 1]/(\overline{\lambda p^2})$. The quantity is constructed to give the first Taylor coefficient in an expansion of the MG density in the parameter $\overline{\lambda p^2}$, when approaching the limit $\overline{\lambda p^2} = 0$ [cf. Eq. (34)]. The line dividing the HO and FE domains in the parameter space is also shown. An oscillatory behavior that is connected to the energy-band structure is visible in the HO domain (cf. Fig. 6).

From the data in the FE-like domain the expansion of Eq. (34) is confirmed with $a_1 = -1/2$ (Fig. 7).

Obtaining a_1 in the HO model

The independent HO expressions [Eqs. (25), (26), and Appendix C] are used to compare the behavior of the HO model with the behavior in the HO-like domain of the MG. The MG model should approach the HO model when $\overline{\lambda}/\overline{p^2} \to \infty$, because the effective potential approaches a harmonic

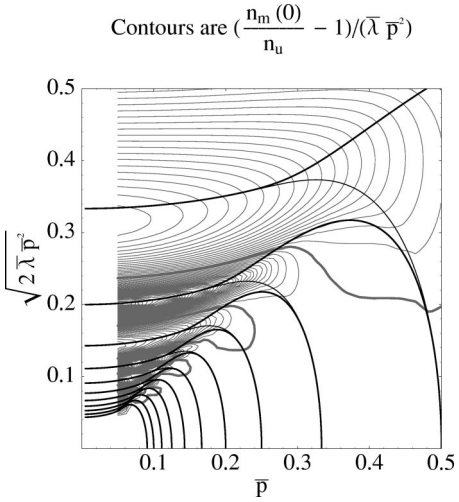

FIG. 6. The density deviations of the MG superimposed by the energy-band structure. The lighter contour lines are the same quantity as shown in Fig. 5. The darker contour lines reproduce the band edges in the MG energy-band structure, as shown in Fig. 3. A dependence of the density deviations on the energy structure is evident.

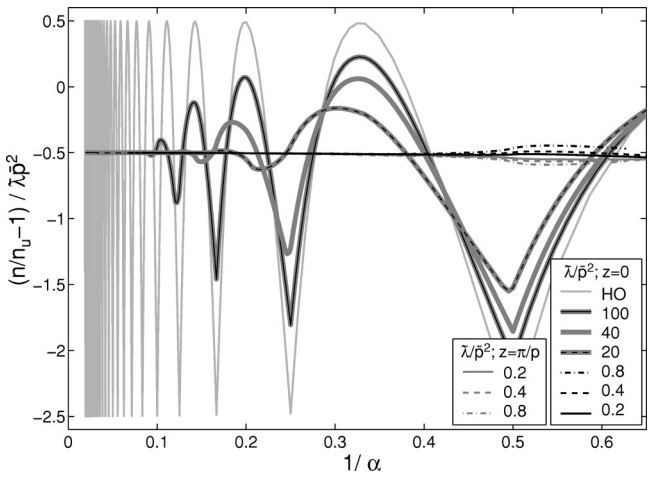

FIG. 7. Density deviations vs $1/\alpha$ for the curves through the parameter space of the MG with constant $\overline{\lambda}/\overline{p^2}=0.2$, 0.4, 0.8, 20, 40, and 100 (shown in legends), corresponding to the long-dashed lines in Fig. 3. The lighter lines with $\overline{\lambda}/\overline{p^2}=0.2$, 0.4, and 0.8 show density deviations in the maximum point $z=\pi/p$, while the other curves show the density deviations in the minimum point $z=0$. The light oscillatory curve shows the density deviations for the HO model, corresponding to the limit $\overline{\lambda}/\overline{p^2}\to\infty$. The parameter α is related to the energy-band structure and is defined in Eq. (29). The slowly varying limit is approached as $1/\alpha\to 0$. In that limit we find $a_1=-0.5$ [cf. Eq. (38)].

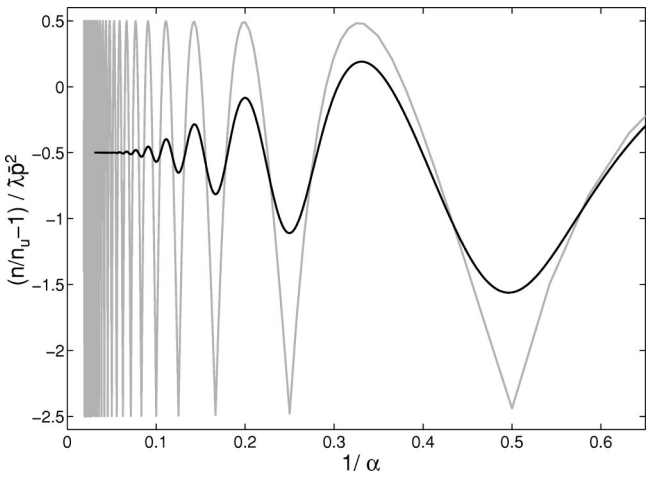

FIG. 8. The black line is the density deviation for the HO model of a system with a low temperature $k_BT=0.05\mu$. The light line is the density deviation for the HO model at $k_BT=0$. In the slowly varying limit we find $a_1=-0.5$ at nonzero temperature, which agrees with the value extracted in Fig. 7.

oscillator potential. Furthermore, in this limit, the MG energy spectrum approach the energy spectrum of the HO system. Hence the MG density in the HO-like limit should approach the pure HO density. This is confirmed in Fig. 7. However, using the limiting procedure in Eq. (38), convergence to a single value of a_1 is not obtained. The convergence is prevented by heavy oscillations, a situation similar to $\sin(1/x)$ in the limit $x\to 0$, with a range of limiting values.

The sum in the expression for the density, Eq. (A1), can be evaluated explicitly at $z=0$, yielding

$$n_h(0)=n_u\sqrt{\pi}\left(\sqrt{2\overline{\lambda}\overline{p^2}}\right)^{3/2}\times\frac{(3/\sqrt{2\overline{\lambda}\overline{p^2}}-4N_e+1)N_e}{4^{N_e}}\frac{(2N_e)!}{(N_e!)^2}. \quad (39)$$

N_e is the number of discrete energy levels with even index n and energy $\epsilon_n\leqslant\mu$. Examining Fig. 7, a periodic behavior with $\Delta\alpha=2$ is seen, where maxima and minima of the oscillations in the density coincide with integer values of α, indicating a strong relationship between the oscillations and the energy-band structure. The limit $\overline{\lambda}\overline{p^2}\to 0$ is therefore taken separately for each point with a fixed relative position to two consecutive even α. By defining a number $0\leqslant\alpha_e<2$ as the smallest number to subtract from α to obtain an even integer (i.e., α_e is the distance in α from the chemical potential, μ, to the highest even energy level $\leqslant\mu$), N_e can be expressed as

$$N_e=\frac{\alpha-\alpha_e}{2}+1, \quad (40)$$

which is inserted into Eq. (39). Using the explicit expression for α for the HO, Eq. (30), and keeping α_e constant, a Taylor expansion of n_h in $\sqrt{2\overline{\lambda}\overline{p^2}}$ gives as coefficient for the term proportional to $\overline{\lambda}\overline{p^2}$,

$$a_1(\alpha_e)=-\frac{5}{2}+6\alpha_e-3\alpha_e^2. \quad (41)$$

This is a parametrization, in α_e, of the range of possible limiting values of a_1.

Averaging $a_1(\alpha_e)$ over $0\leqslant\alpha_e<2$ gives $-1/2$, i.e., the same value of a_1 as extracted from the FE domain of the MG. Oscillations in the HO model are thus superimposed on a curve converging to the same value of a_1 as in the FE domain.

When a low temperature is introduced by adding the usual temperature factors[26] into the KS-orbital system and numerically recalculating the density, a_1 converges to $-1/2$, as is seen in Fig. 8. This motivates taking averages over α_e in the zero-temperature HO model, or equivalently, averaging over the position of the chemical potential in the energy-band structure, as a way of extracting information valid in more realistic cases.

To summarize, the density of the MG model behaves differently in the FE-like and HO-like regions of the parameter space. In the first region the chemical potential is in a FE-like energy structure. The density is well behaved, and converges to $a_1=-1/2$. In the second region the chemical potential is in a HO-like discrete z-dimension energy structure. The density oscillates heavily with the system parameters. Curves with $\overline{\lambda}/\overline{p^2}$ constant, starting from the HO-like region and approaching the slowly varying limit (by going in the limit $\overline{\lambda}\overline{p^2}\to 0$) eventually reach the FE-like region where the oscillations damp out. In the case of the pure HO system,

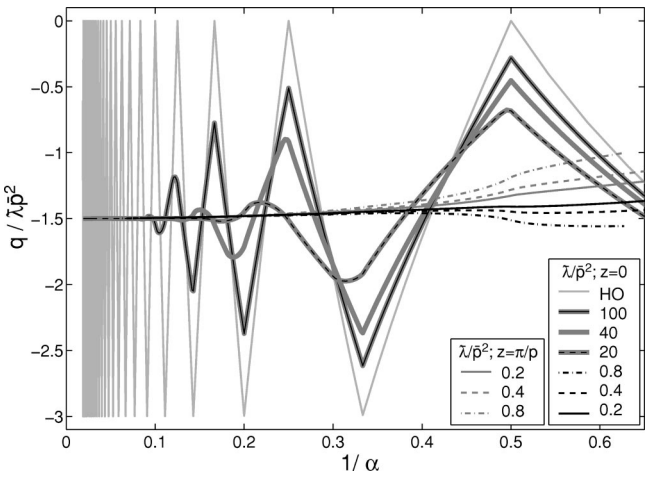

FIG. 9. Laplacian deviations $q/(\overline{\lambda p^2})$ vs $1/\alpha$ for the same parameters as in Fig. 7. In the slowly varying limit we find $a_2 = -1.5$ [cf. Eq. (42)].

however, the chemical potential is stuck between the endless number of purely discrete energy levels, leaving the oscillations undamped.

The oscillations present in the HO model (and throughout the HO-like domain of the MG) are a technical issue at zero temperature and uninteresting when drawing conclusions about more realistic systems. When introducing a temperature into the HO model, or, equivalently, averaging over the position of the chemical potential, the limiting value of $a_1 = -1/2$ is recovered. Note that no artificial finite size is imposed in our calculations, like using periodic boundary conditions or hard walls. The oscillations emerge naturally from the discrete energy levels in the HO limit and are present also in the non-numerical treatments. Hence, when using such a simplistic model as the HO to test proposed gradient expansions or for fitting of parameters, some method similar to our α averages or temperature additions must be used to quench the oscillations and obtain results valid for general systems.

C. Determination of the coefficient of Laplacian deviation, a_2

Next, we examine

$$\frac{q_m(0)}{\overline{\lambda p^2}} \xrightarrow{\overline{\lambda p^2}\to 0} a_2, \tag{42}$$

where $a_2 = -3/2$ in the FE-like part of parameter space (Fig. 9).

Obtaining a_2 in the HO model

In the HO model, the Laplacian of the density has an oscillatory behavior similar to that of the density, as seen in Fig. 9. For $z=0$, the Laplacian, Eq. (11), for the HO model becomes

$$q_h(0) = \frac{4c_q}{15}\frac{(5/\sqrt{2\overline{\lambda p^2}} - 12N_o - 3)(2N_o^2 + N_o)}{4^{N_o}}\frac{(2N_o)!}{(N_o!)^2} - \frac{8c_q}{15}\frac{(5/\sqrt{2\overline{\lambda p^2}} - 12N_e - 1)(N_e^2 - N_e)}{4^{N_e}}\frac{(2N_e)!}{(N_e!)^2} - \frac{2c_q}{3}\frac{(3/\sqrt{2\overline{\lambda p^2}} - 4N_e + 1)N_e}{4^{N_e}}\frac{(2N_e)!}{(N_e!)^2}, \tag{43}$$

$$c_q = \left(\frac{n_u}{n_h(0)}\right)^{5/3}\frac{3\sqrt{\pi}}{4}(\sqrt{2\overline{\lambda p^2}})^{5/2}. \tag{44}$$

N_e is the number of discrete energy levels with even index n, and N_o is the number of discrete energy levels with odd index m, such that their energies ϵ_n and $\epsilon_m \leqslant \mu$.

In analogy to α_e above, we introduce a parameter $0 \leqslant \alpha_o < 2$ as the smallest number that gives an odd integer when it is subtracted from α. We get

$$N_o = \frac{\alpha - \alpha_o}{2} + \frac{1}{2}. \tag{45}$$

The relation between α_o and α_e is ($\{x\}$ denotes the decimal part of x)

$$\alpha_o = 2\left\{\frac{\alpha_e + 1}{2}\right\}. \tag{46}$$

Thus, if α_e is constant, α_o must also be constant. This relation is based on the equal spacing of the HO energy levels and thus is only valid in the pure HO model.

Using $N_o(\alpha_o)$ and $N_e(\alpha_e)$ and keeping α_e and α_o constant, a Taylor expansion of Eq. (43) in $\sqrt{2\overline{\lambda p^2}}$ gives the coefficient for the term proportional to $\overline{\lambda p^2}$ as

$$a_2(\alpha_e) = -3(1 - |\alpha_e - 1|), \tag{47}$$

where we have eliminated α_o by observing that α_e and α_o fulfill $1 + (1-\alpha_o)^2 - (1-\alpha_e)^2 = 2(1 - |\alpha_e - 1|)$ in the interval of their definition. Averaging $a_2(\alpha_e)$ over $0 \leqslant \alpha_e < 2$ gives $-3/2$, i.e., the same as the value of a_2 in the FE-like domain of the MG.

D. Divergence of the coefficient of exchange energy per particle deviation, a_3

When examining

$$\frac{[\epsilon_{x,m}^{\mathrm{irxh}}(0)/\epsilon_{x,u}^{\mathrm{irxh}} - 1]}{\overline{\lambda p^2}} \xrightarrow{\overline{\lambda p^2}\to 0} a_3, \tag{48}$$

as in Fig. 10, no convergence to a value a_3 in the limit $\overline{\lambda p^2} \to 0$ is observed. This indicates that $\epsilon_{x,m}^{\mathrm{irxh}}(0)$ does not have an analytical expansion in $\overline{\lambda p^2}$, as was assumed in Eq. (36). In Fig. 10 the same expression but with the LDA exchange energy per particle is also shown. As expected the LDA limiting value is $a_1/3 = -1/6$, which is obtained by inserting Eq. (34) into Eq. (8).

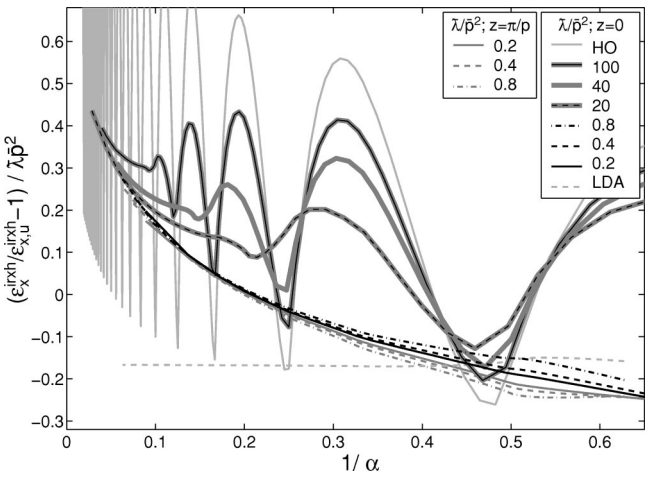

FIG. 10. Deviations from the uniform electron gas exchange energy per particle, $(\epsilon_x^{\mathrm{irxh}}/\epsilon_{x,u}^{\mathrm{irxh}}-1)/(\overline{\lambda p^2})$, for the same parameters as in Figs. 7 and 9. In the slowly varying limit this expression is expected to approach the a_3 coefficient in Eq. (48), but all irxh curves are diverging and no value can be extracted. For comparison the same expression for the LDA exchange energy per particle, $(\epsilon_x^{\mathrm{LDA}}/\epsilon_{x,u}^{\mathrm{irxh}}-1)/(\overline{\lambda p^2})$ for $\overline{\lambda}/\overline{p^2}=0.8$, is shown.

a_3 *in the HO model*

In the HO model, not only the characteristic energy structure related oscillations are present but also the divergence seen in the FE-like domain of the MG (Fig. 10). Since both the maxima and the minima diverge in the $\overline{\lambda p^2}\to 0$ limit, the averaging technique used previously would not cure the divergence. Nor will the behavior be canceled by the other coefficients when composing b^{irxh} according to Eq. (37).

The divergence of the a_3 coefficient does not imply that $\epsilon_{x,h}^{\mathrm{irxh}}$ itself diverges. In fact, $\epsilon_x^{\mathrm{irxh}}$ converges to the FE-limit of Eq. (33) in both the MG and the pure HO. This indicates that $\epsilon_x^{\mathrm{irxh}}$ is not analytical at all points, which we will discuss in a later section. The divergence in the limit $\overline{\lambda p^2}\to 0$ with $\overline{\lambda}/\overline{p^2}$ constant, seems to be of logarithmic kind (rather than, for example, x^y with y being a fractional number). It could be possible to create a local expansion of such a nonanalytical function, but not as a regular power expansion as Eq. (14). A suitable expansion needs one or more nonanalytical terms that tend to zero in the slowly varying limit, like $q\log|q|$.

E. Analyzing data at the maximum of the potential

The fact that the gradient term in the expansion in Eq. (14) is zero at the minimum of the potential at $z=0$ was used above, thus giving direct access to the value of b^{irxh}. This is also the case at the maximum of the potential at $z=\pi/p$, which allows us to analyze the results in terms of negative curvature.

We must, however, compare with the correct uniform electron gas, having a chemical potential $\mu_{\max}=\mu-2\lambda$. Thus $k_{F,u}$ in Eqs. (32) and (33) should be replaced by $(k_{F,u})_{\max}=k_{F,u}\sqrt{1-2\overline{\lambda}}$, and the negative dimensionless curvature must be rescaled according to $(\overline{\lambda p^2})_{\max}=-\overline{\lambda p^2}(1-2\overline{\lambda})^{-2}$.

Since the limiting procedure of low curvature at the maximum point is appropriate only for chemical potentials $\mu>2\lambda$, or $\overline{\lambda}<1/2$, data outside the FE-like part of the parameter space of the MG are not investigated (Fig. 3).

The three quantities to consider thus are

$$\frac{n_m(z=\pi/p)/[n_u(\sqrt{1-2\overline{\lambda}})^3]-1}{-\overline{\lambda p^2}(1-2\overline{\lambda})^{-2}}, \tag{49}$$

$$\frac{q_m(z=\pi/p)}{-\overline{\lambda p^2}(1-2\overline{\lambda})^{-2}}, \tag{50}$$

$$\frac{\epsilon_{x,m}^{\mathrm{irxh}}(z=\pi/p)/(\epsilon_{x,u}^{\mathrm{irxh}}\sqrt{1-2\overline{\lambda}})-1}{-\overline{\lambda p^2}(1-2\overline{\lambda})^{-2}}. \tag{51}$$

In Figs. 7, 9, and 10 the data for the maximum points are drawn as light lines. No major differences are seen between darker and lighter lines, confirming the symmetry between positive and negative curvature in the density and the Laplacian, and implying this symmetry for the inverse radius of the exchange hole definition of the exchange energy per particle, Eqs. (4)–(7), at low curvature.

V. COMMENTS ON NUMERICAL RESULTS

Since we only have numerical proof that b^{irxh} is not well defined, indicating nonanalyticity of the exchange energy per particle of Eqs. (4)–(7), the accuracy of our results needs to be considered. As seen in Fig. 10, LDA has converged well before the irxh curves are in doubt numerically, which is one indication that the divergence of the irxh curves is not due to numerical errors. We base an estimate of the accuracy of our calculations in the FE-like domain of the MG on an independent numerical inspection which will be explained in this section. The estimated errors are presented in Table I.

Not only the prefactor 10/81 in Eq. (9) is known but also prefactors for higher-order terms.[27] While remembering that these factors are valid only as an expansion of the exchange energy itself, that is, for the expansion integrated together with the density according to Eq. (2), we use this as an independent check of the accuracy of our numerical calculations of the exchange energy per particle.

The fourth-order expansion is according to Svendsen and von Barth (SvB),

$$\epsilon_x^{\mathrm{SvB}}=\epsilon_x^{\mathrm{LDA}}\left(1+\frac{10}{81}s^2+\frac{146}{2025}q^2-\frac{73}{405}s^2q+0s^4\right). \tag{52}$$

The higher-order prefactors 73/405 and 0 are not exact but the possible errors in these prefactors does not influence the results since s and q are very small in the FE-like domain of the MG. For values in the HO-like domain, s and q can be very large and a comparison with the SvB expression is not adequate.

In Fig. 11 $\epsilon_x^{\mathrm{SvB}}/\epsilon_x^{\mathrm{LDA}}$ and $\epsilon_x^{\mathrm{irxh}}/\epsilon_x^{\mathrm{LDA}}$ are compared over a half period in the spatial coordinate for one representative set

TABLE I. Error estimates for selected points in Fig. 10. The right part of the table refers to Fig. 3 for the location of the point in the parameter space and to Fig. 11 for the error estimates. The difference Δ between the value of $\epsilon_x^{\mathrm{irxh}}/\epsilon_x^{\mathrm{LDA}}$ in $\overline{z}=0$ and $\overline{zp}=\pi/2$ is included in the table as a measure of the scale on the y axis in Fig. 11. By adding $\delta(\epsilon_x^{\mathrm{irxh}}/\epsilon_x^{\mathrm{LDA}})$ to the calculated data, the same total exchange energy is obtained as with the SvB expansion, Eq. (52); see Sec. V and Fig. 11. This corresponds to adding $\delta(\epsilon_x^{\mathrm{irxh}}/\epsilon_{x,u}^{\mathrm{irxh}})/\overline{\lambda p^2}$ to the points in Fig. 10. The third column shows errors for points on the data curves for minima, while the fourth column shows errors for points on the data curves for the maxima.

$\overline{\lambda}/\overline{p^2}$	$1/\alpha$	$\delta\left(\frac{\epsilon_x^{\mathrm{irxh}}(0)}{\epsilon_{x,u}^{\mathrm{irxh}}}\right)/\overline{\lambda p^2}$	$\delta\left(\frac{\epsilon_x^{\mathrm{irxh}}\left(\frac{\pi}{\overline{p}}\right)}{(\epsilon_{x,u}^{\mathrm{irxh}})_{\max}}\right) \Big/ (\overline{\lambda p^2})_{\max}$	$\overline{p}$	Δ	$\delta\left(\frac{\epsilon_x^{\mathrm{irxh}}}{\epsilon_x^{\mathrm{LDA}}}\right)$
0.2	0.596	-0.0002	0.0002	0.553	-2.179×10^{-3}	-4×10^{-6}
0.2	0.089	-0.0116	0.0115	0.089	8.842×10^{-6}	-1.45×10^{-7}
0.8	0.582	0.0007	-0.0003	0.494	-8.035×10^{-3}	3.5×10^{-5}
0.8	0.097	-0.0012	0.0012	0.096	4.692×10^{-5}	-8×10^{-8}
0.8	0.062	0.0113	-0.0112	0.062	10.356×10^{-6}	1.35×10^{-7}
20	0.075	0.0007	N/A	0.071	5.091×10^{-4}	3×10^{-7}
20	0.044	0.0024	N/A	0.043	7.656×10^{-5}	1.6×10^{-7}
100	0.080	0.0155	N/A	0.061	5.262×10^{-3}	2.2×10^{-5}

of values of $\overline{\lambda}$ and $\overline{p}$. It is obvious that these two quantities can only be compared via the integrated values according to the exchange part of Eq. (2).

The errors in our data points are estimated by comparing the different integrated values, making the following assumptions: (i) The numerical errors in the calculation of the density are negligible, compared with the errors made in the calculation of the exchange energy per particle, since the density calculation is much less complex [compare Eqs. (B2) and (B3)]. The density is also well behaved as seen in Fig. 7.

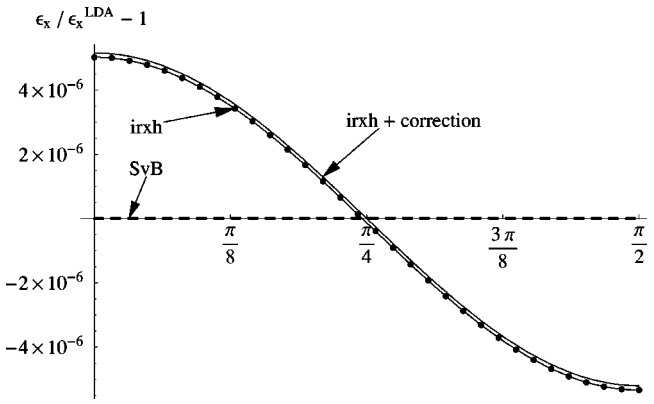

FIG. 11. Exchange functionals based on different sets of definitions can only be compared via the total exchange energy given by the exchange part of Eq. (2). This is evident in the figure where the SvB exchange energy per particle from Eq. (52) is shown together with the irxh exchange energy per particle in Eqs. (4)–(7) over a half period in the spatial coordinate for $\sqrt{2\overline{\lambda p^2}}=0.0049$ and $\overline{p}=0.0621$. In order to obtain the same total exchange energy from the SvB and the irxh exchange energy per particle a uniform correction of 1.35×10^{-7} is needed for the irxh. This is shown with the full line. The exchange energy obtained from the SvB expansion in Eq. (52) can be considered exact because of the small parameters used in this work.

This implies that the value of the total exchange energy based on the SvB expansion in Eq. (52) can be considered an exact reference value as long as s and q are small. (ii) Statistical errors, due to limited internal numerical precision in the computer, are negligible compared with systematic errors. This is based on the smoothness of the curve joining consecutive points in Fig. 11. If there was a statistical error, the points would be scattered in a band of a width corresponding to the statistical error. (iii) The systematic error is the same over the entire interval shown in Fig. 11. We have found no reason why the systematic error should have a dependence on position. The full line in Fig. 11 was created by adding a uniform systematic error to the $\epsilon_x^{\mathrm{irxh}}/\epsilon_x^{\mathrm{LDA}}$ curve chosen to make this curve give the same value of the total exchange energy as obtained from the $\epsilon_x^{\mathrm{SvB}}/\epsilon_x^{\mathrm{LDA}}$ curve.

As a further indication that the discovered behavior is correct we note that the two model systems, the MG and the HO, have been treated separately (see Appendixes B and C) and the divergence is present in both models.

VI. DISCUSSION AND CONCLUSIONS

In the first part of this work we discussed a way, via subsystem functionals, of extending the successful use of DFT to more complex systems than are addressed today. The basic idea of subsystem functionals is to apply different functionals to different parts of a system. This puts the additional constraint on the functionals that they all must adhere to a single explicit choice of the exchange-correlation energy per particle. A limited subsystemlike scheme has already been implemented and tested.[7]

To make the scheme of subsystem functionals competitive with current multipurpose functionals, a subsystem functional more accurate than LDA for the slowly varying interior part of a system is needed. We address the derivation of such a functional in the second part of this work by examin-

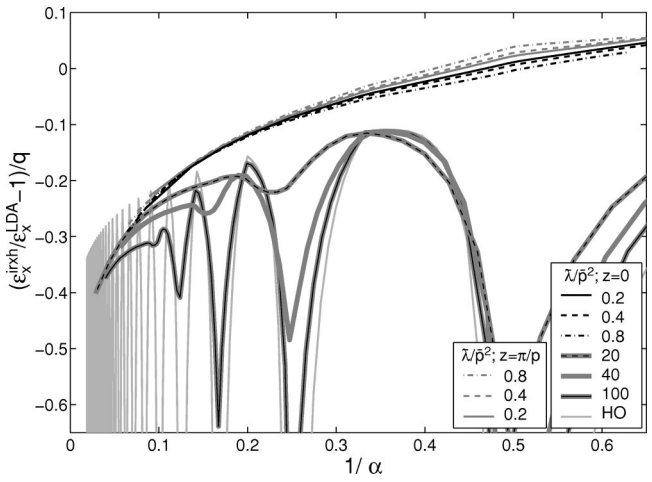

FIG. 12. The quantity $(\epsilon_x^{\mathrm{irxh}}/\epsilon_x^{\mathrm{LDA}}-1)/q$ vs $1/\alpha$ for the same parameters as in Figs. 7, 9, and 10, summarizing the data presented in these plots. In the limit of slowly varying densities, $1/\alpha \to 0$, this quantity is expected to approach the Laplacian coefficient of the conventional (irxh) exchange energy per particle, b^{irxh}, but the divergence found in Fig. 10 prevents convergence and thus no such coefficient exist. We thus conclude, in Sec. VI, that the irxh exchange energy per particle can not be expanded in the density variation as suggested in Eq. (14), which indicates that it is not a good choice when deriving subsystem functionals, which need to adhere to an explicit choice used throughout the whole system.

ing the conventional definition of the exchange energy per particle, Eqs. (4)–(7), for two specific model systems, the MG and the HO. We arrive at the general result that an expansion of this exchange energy per particle in the density variation must contain a nonanalytical function of the dimensionless Laplacian (if such an expansion exists at all). Our numerical results, presented in Figs. 7, 9, and 10, can be summarized as in Fig. 12.

Any attempt to model the exchange energy per particle defined by Eqs. (4)–(7) with an analytical expression will be futile, in the sense that it will be unable to reproduce the nonanalytic behavior found in the slowly varying limit of the MG. This issue needs to be considered also outside the context of subsystem functionals, particularly when Laplacian terms are included in GGA-type functionals. The general scheme of subsystem functionals is unaffected by the nonanalyticity, but it makes the construction of a subsystem functional for systems with slowly varying densities less straightforward. Most importantly it indicates that the conventional (irxh) definition of the exchange energy is not a good choice for the derivation of subsystem functionals.

The established nonanalytical behavior is consistent throughout the wide variety of systems encompassed by the MG model. The MG includes both the finite system of the HO and the extended system of the weakly perturbed periodic potential, two very dissimilar systems. A functional based on the results for the MG can potentially become a true multipurpose functional useful for atoms, molecules, and bulk systems.

Nonanalytical behavior and improper coefficients have appeared in previous work[28] regarding the same exchange energy per particle, but only in such a way that it is unknown whether the difficulties found were caused by problems with the exchange energy per particle or due to other issues (such as in which order the limits have been taken). In contrast, our results show how the unscreened, zero-temperature expressions themselves raise difficulties.

We suspect the long Coulomb tails to be responsible for the nonanalytic behavior of the exchange energy per particle. The nonanalyticity should disappear if screening is introduced. This can be done by using a Yukawa potential in place of the Coulomb potential in Eq. (5). Another way of taking the screening into account is to perform a full random-phase approximation (RPA) calculation.

In conclusion, we have found that for the creation of an expansion for subsystem functionals of the exchange energy per particle in the density variation, i.e., to go beyond the LDA exchange in a subsystem, there are two options. Either the nonanalytical function of the dimensionless Laplacian must be found and included in a density functional based on the irxh exchange energy per particle, Eqs. (4)–(7), or an alternative definition of the exchange energy per particle must be chosen. Alternative definitions have been suggested[10] and we plan to continue our investigation by examining if any of these can give an exchange energy per particle that can be expanded in a Taylor series. Note, however, that most (if not all) of the exact conditions that are used when constructing an exchange functional in the traditional way are based on the definition in Eqs. (4)–(7). New similar conditions need to be constructed if another definition is used. Some such conditions on alternative definitions have already been derived.[29] As a final remark we note that the origin of the division of the exchange-correlation energy into an exchange and a correlation part is based on the Hartree-Fock method that treats exchange only. In DFT this division is artificial. An alternative way to proceed could be to either divide the exchange-correlation energy in another way or to not divide it at all.

ACKNOWLEDGMENTS

We thank Walter Kohn, John Perdew, Ulf von Barth, Stefan Kurth, and Thomas Mattsson for fruitful discussions. We also want to thank Saul A. Teukolsky who kindly proposed a good method for calculating the Mathieu functions. Parts of the calculations where done on the IBM SP computer at PDC in Stockholm. Financial support from the Göran Gustafsson Foundation is gratefully acknowledged. This work was partly funded by the project ATOMICS at the Swedish research council SSF. Sandia is a multiprogram laboratory operated by Sandia Corporation, a Lockheed Martin Company, for the United States Department of Energy under Contract No. DE-AC04-94AL85000.

APPENDIX A: GENERAL COMPUTATIONAL FORMULAS

The density and the inverse radius of the exchange hole, defined in Eqs. (1) and (5) respectively, are computed according to the formulas in Ref. 6 where the x and y dimensions in both real and reciprocal space are integrated out. For

completeness these formulas are restated here, in a more general form,

$$n(z)=2\sum_{\eta}|\varphi_{\eta}|^2 w_{\eta},\quad w_{\eta}=\frac{m}{2\pi\hbar^2}(\mu-\epsilon_{\eta}) \tag{A1}$$

and

$$\epsilon_x^{\mathrm{irxh}}(\mathbf{r})=-\frac{e^2}{2\pi n(z)}\int dz'\sum_{\eta}\sum_{\eta'}\varphi_{\eta}(z)\varphi_{\eta}^*(z')\varphi_{\eta'}^*(z)\times\varphi_{\eta'}(z')(\Delta z)^{-3}g(k_{\eta}\Delta z,k_{\eta'}\Delta z), \tag{A2}$$

$$g(r,r')=rr'\int_0^{\infty}\frac{J_1(rt)J_1(r't)}{t\sqrt{1+t^2}}dt, \tag{A3}$$

where $k_{\eta}=[2m(\mu-\epsilon_{\eta})/\hbar^2]^{1/2}$; $\Delta z=|z-z'|$; and the sums in Eqs. (A1) and (A2) should be taken over all η of occupied orbitals in the zero-temperature ground state.

Calculation of $g(r,r')$

To calculate numerical values of $g(r,r')$ a method for calculating Bessel functions, $J_1(x)$ is needed. We use the algorithm described in Ref. 30, as implemented in Ref. 31, but extended with coefficients for higher accuracy.

The $g(r,r')$ function has a long oscillating tail, which is handled by separating it into two terms:

$$\frac{g(r,r')}{rr'}=\int_0^{\infty}\frac{J_1(rt)J_1(r't)}{t^2}dt+\int_0^{\infty}J_1(rt)J_1(r't)\times\left(\frac{1}{t\sqrt{t^2+1}}-\frac{1}{t^2}\right)dt. \tag{A4}$$

The first part can be integrated for $r>r'$, giving [with $K(z)$ and $E(z)$ as the complete elliptic integrals of the first and second kind[24]]

$$\int_0^{\infty}\frac{J_1(rt)J_1(r't)}{t^2}dt=\frac{2}{3r'\pi}\left[(r^2+r'^2)E\left(\frac{r'^2}{r^2}\right)-(r^2-r'^2)K\left(\frac{r'^2}{r^2}\right)\right]. \tag{A5}$$

The special case $r=r'$ gives

$$\int_0^{\infty}\frac{J_1^2(rt)}{t^2}dt=\frac{4r}{3\pi}. \tag{A6}$$

The complete elliptic integrals are calculated using the implementations of Ref. 31, modified for higher accuracy. Numerical integration is still needed for the second integral in Eq. (A4), but the oscillations of this integrand decay much faster than the oscillations in the original integrand, and hence are easier to handle.

The infinite interval of integration is treated by introducing an error bound ϵ and setting it equal to an approximation of the tail integral. The approximation is created by composing a new integrand from the asymptotic behaviors of the integrated functions,

$$J_1(rt)\xrightarrow{t\to\infty}-\sqrt{\frac{2}{\pi rt}}\cos\left(rt-3\frac{\pi}{4}\right), \tag{A7}$$

$$\frac{1}{t\sqrt{1+t^2}}-\frac{1}{t^2}\xrightarrow{t\to\infty}-\frac{1}{2t^4}, \tag{A8}$$

but leaving out the cosine as it only superimposes oscillations and is $\leqslant 1$. When integrating this expression from t_0 to infinity it gives an approximation of the tail integral, which is solved for t_0 to give a value for where to end the integration over t:

$$t_0=\frac{1}{(4\pi\epsilon\sqrt{rr'})^4}. \tag{A9}$$

Details on the method used for the numerical integration are found in Appendix B4.

The speed of the calculation is increased with a lookup table for $g(r,r')$. Bicubic interpolation is used, with three million lookup points for values of r and r' ranging from 0 to 1200. The points are distributed with a nonlinear transformation to increase accuracy for very small r,r' and when r is almost equal to r'. There is a limiting expression for $g(r,r')$ for large values of r and $r'<r$ that could have been useful for the construction of the lookup table:

$$g(r,r')\xrightarrow{r\to\infty}\left(\frac{1}{2}-\frac{1}{\pi r}\right)r'^2, \tag{A10}$$

but this expression has a relative error of as large as 10^{-4} at the highest values of r needed in our calculation (about 1000). Since the calculations required a higher precision the expression is not used.

APPENDIX B: COMPUTATIONAL FORMULAS FOR THE MG

There is a simple relation between the form of Mathieu functions used here, the $F_{\eta}(z)$ of Eq. (18), and the real even and odd forms of the Mathieu functions,[24] *ce* and *se*, which are commonly found in numerical software. Although we compute $F_{\eta}(z)$ directly, this relationship is useful for making independent verifications:

$$F_{\eta}(z)=ce_{\eta}\left(z,-\frac{1}{2}\frac{\overline{\lambda}}{\overline{p^2}}\right)+ise_{\eta}\left(z,-\frac{1}{2}\frac{\overline{\lambda}}{\overline{p^2}}\right). \tag{B1}$$

It was shown in Sec. III A that η enumerates the solutions of different energies, giving a rudimentary band structure. When L_3 of Eq. (18) approaches infinity, η can take any value from $-\tilde{\eta}$ to $\tilde{\eta}$, where $\tilde{\eta}$ is the positive number enumerating the state with largest energy $\epsilon_{\tilde{\eta}}\leqslant\mu$. The energy ϵ_{η} is a continuous function of η except at integers, and can be integrated numerically if formulas that exclude the discon-

tinuous points are used. Besides the practical issues, the discontinuities of ϵ_η have no influence on the values of the integrals, as they only occur at a finite number of single points.

The KS orbitals in Eq. (18) can be used to express the density and the irxh exchange energy per particle as

$$n_m(z) = n_u \frac{3}{2} \int_0^{\tilde{\eta}} |F_\eta(\overline{pz})|^2 \left(1 - \frac{\epsilon_\eta}{\mu}\right) d\eta, \tag{B2}$$

$$\epsilon_{x,m}^{\mathrm{irxh}}(z) = \epsilon_{x,u}^{\mathrm{irxh}} 2\overline{p}^2 \frac{n_u}{n_m(\overline{z})} \int_{-\infty}^{\infty} d\overline{z'} \int_0^{\tilde{\eta}} d\eta \int_0^{\tilde{\eta}} d\eta' \times \mathrm{Re}[F_\eta(\overline{pz}) F_\eta^*(\overline{pz'})] \mathrm{Re}[F_{\eta'}^*(\overline{pz}) F_{\eta'}(\overline{pz'})] \times (\Delta\overline{z})^{-3} g(\overline{k}_\eta \Delta\overline{z}, \overline{k}'_\eta \Delta\overline{z}), \tag{B3}$$

$$\overline{k}_\eta = \sqrt{1 - \epsilon_\eta/\mu}, \tag{B4}$$

where $\Delta\overline{z} = |\overline{z} - \overline{z'}| = k_F \Delta z$, and we have used $F_{-\eta}(z) = F_\eta^*(z)$.

Important issues with the computation of these formulas will be treated in the subsections below.

1. Mathieu functions

The algorithm for computing Mathieu functions presented here has similarities with the one presented in Ref. 32, but the code was developed by us. In Sec. III A a Fourier expanded Floquet solution was inserted into the Mathieu differential equation, giving a matrix eigenvalue equation describing the solutions, Eq. (19). To solve this equation numerically the matrix must be truncated at some finite size $2K+1$. We based the choice of K for a given η on the numerical testing performed in Ref. 32. The eigenvalue problem is solved by regular numerical methods, using the algorithms from Ref. 31. (We are aware that these implementations are not as efficient and optimized as more specialized routines.)

The index η can be parted into a sum of two terms, an even integer and a reduced index $-1 < \zeta \leqslant 1$, as discussed in Sec. III A. Solutions with the same ζ, but with different even integer parts, show up as solutions with different eigenvalues $a(\eta, \overline{\lambda}/(2\overline{p}^2))$ to the same matrix problem. Solutions for negative η are obtained from the relabeling $c_{2k}^{\eta} \rightarrow c_{-2k}^{\eta}$. Hence one single solution of the matrix eigenvalue problem produces values for all $\eta =$ even number $\pm|\zeta|$.

The routines for the Mathieu functions are also used to determine $\tilde{\eta}$ from a known chemical potential μ using the bisection method. Guesses of $\tilde{\eta}$ are refined until an energy as close to μ as possible is obtained. There are more efficient ways of determining $\tilde{\eta}$ from μ, but since this is only done once per computed data point, the time lost by using bisection is negligible.

2. Integrations over the Mathieu index η

One solution to the Mathieu matrix equations produces values for all Mathieu functions with $\eta =$ even number $\pm|\zeta|$. Because of this, but also as a way to handle the discontinuities of ϵ_η when η is integer, the integrations over η are parted up (using $\tilde{\zeta}$ as the reduced index of $\tilde{\eta}$):

$$\int_0^{\tilde{\eta}} f(\eta) d\eta = \int_0^{|\tilde{\zeta}|} \left(\sum_{i=0}^{A} f(2i+\zeta) + \sum_{i=1}^{B} f(2i-\zeta) \right) d\zeta + \int_{|\tilde{\zeta}|}^{1} \left(\sum_{i=0}^{C} f(2i+\zeta) + \sum_{i=1}^{D} f(2i-\zeta) \right) d\zeta. \tag{B5}$$

For a given $\tilde{\eta}$, values for A, B, C, and D must be carefully chosen to make the right-hand expression constitute the whole interval 0 to $\tilde{\eta}$. Details on the method used for the numerical integration are found in Sec. B4.

3. Infinite integration over $\overline{z'}$

The integrand over $\overline{z'}$ in Eq. (B3) is the expression for the exchange hole divided by a positive distance and thus always has the same sign. Furthermore, the doubly infinite integration over all $\overline{z'}$ is split at $\overline{z}$, transformed and re-added into one integration from 0 to infinity, giving slightly more complicated arguments in the Mathieu functions.

To handle the infinite interval of integration it is possible to extract a limiting behavior for the $\overline{z'}$ integral for the uniform electron gas (the same cannot be done for the MG), giving a result proportional to $1/\overline{z'}^3$. This result, and numerical experiments throughout the parameter space of the MG, indicate that this is an upper limit on how slowly the oscillations in the integrand can decay. In the HO-like area of the MG the oscillations die out much more quickly. When approaching the FE limit the decay of the oscillations approaches the result found for the uniform electron gas. Based on this, our method to handle the z integration is to fit a function of the form $\mathrm{const}/\overline{z'}^3$ to the behavior of the last part of the integrand. As the integrand decays like this fitted function or more quickly, and has a constant sign, two approximate values of the total integral appear. The first has the additional $\mathrm{const}/\overline{z'}^3$ tail added, and the second totally disregards any tail contributions. These two values for the integral are approximations of an upper and lower bound on the real value of the integral. The integration of the $\overline{z'}$ integral is halted when these upper and lower bounds are closer than the accuracy goal set for the integration.

4. Method of numerical integration

An integration algorithm suitable for parallel computers is needed, as the multiple levels of integration in the expressions are very time consuming for certain choices of parameters. There are many nonparallel integration routines available, such as the QUADPACK (Ref. 33) routine ''dqag.'' The ''dqag'' routine is intended for integration of oscillatory in-

tegrands, like those encountered in this work. It handles them adaptively in the sense that it spends most of the time on the difficult parts of the integrand. For parallel computers there are only a few commonly available similar adaptive integration routines, as distributing an equal load to each computer node is difficult.

However, for the integrations encountered in this work the gain of a proper adaptive integration method is limited, as the integrands usually are smooth but heavily oscillating, with a frequency not varying much throughout the interval of integration. This motivates the choice of a more basic algorithm refining the entire interval of integration at once, which makes a parallel implementation easier. The algorithm presented here has been developed by us and used in most of the calculations.

As all finite ranges can be substituted into the range from 0 to 1, only this case will be treated. Ordinary integral substitution using a function, $x=w(x')$, fulfilling $w(0)=0$ and $w(1)=1$, gives

$$\int_0^1 f(x)dx = \int_0^1 f(w(x))w'(x)dx. \tag{B6}$$

We seek an explicit expression for $w(x)$ whose right derivatives, to any order, equals zero as $x\to+0$, and whose left derivatives, to any order, equals zero at $x\to 1$. A function fulfilling these requirements is

$$w(x)=\int_0^x ce^{-1/(z-z^2)}dz, \quad w'(x)=ce^{-1/(x-x^2)}, \tag{B7}$$

$$c=\left(\int_0^1 e^{-1/(z-z^2)}dz\right)^{-1}, \tag{B8}$$

where c is chosen to meet the requirement $w(1)=1$.

The integration of the combination $f(w(x))w'(x)$ can now be seen as an integration of one period of a periodic function, as the function values and all derivatives match at $x\to+0$ and $x\to 1$. For such integrands ordinary trapezoid integration converges very rapidly, since error terms cancel. The argument assumes that $f(w(x))w'(x)$ approaches zero in these limits, which is true unless $f(x)$ is too divergent; similar assumptions are also made for the derivatives of $f(x)$.

The combination of this substitution and the trapezoid integration can be recast on a form similar to the one used for Gaussian quadrature formulas (by also using the requirements $\lim_{x\to+0}w'(0)=0$ and $\lim_{x\to 1}w'(1)=0$, the two outermost terms have been disregarded):

$$\int_0^1 f(x)dx \approx h\sum_{n=1}^{1/h-1} v_n f(x_n), \tag{B9}$$

$$x_n=w(hn), \quad v_n=w'(hn), \tag{B10}$$

where h is a chosen step length. For each step length the values of v_n and x_n can be pre-calculated with some other, simple, numerical integration algorithm during the program initialization. For the implementation we note that the two quantities should be stored intermixed in one array to ensure good use of the cache memory of the computer.

The integration is performed by iteration, reducing h in each step, until the relative difference between the results from two consecutive steps is less than some error bound ϵ. A major benefit inherited from the trapezoid integration is that if h is reduced with a factor of 2 in each step, the previous computed approximation for the next iteration can be reused. This halves the number of function evaluations needed.

Despite the fact that Eq. (B9) formally does not include the end points of the interval (i.e., it is formally open), the nature of the function $w(x)$ brings x_1 and x_{n-1} extremely close to 0 and 1 (i.e., for practical purposes the formula is to be regarded as closed). In case the end points of the interval must be avoided, the interval of integration can be shrunk minimally and open trapezoid integration used on these small parts.

For the integrals in this work the described integration algorithm shows both a rapid convergence and a very stable behavior. In tricky situations, where the integrand is not entirely smooth, the algorithm results in a trapezoid integration of a nonperiodic function, and thus converges (although slowly). However, for the cases where the integrand is well behaved and smooth (as it should be), the convergence is much more rapid, imitating the behavior seen with usual trapezoid integration of whole periods of periodic functions. For the nonparallel case the results and speed of the described integration method for integrals relevant for this work were compared with the QUADPACK (Ref. 33) routine ''dqag.'' That routine seems to be significantly slower, requiring on the average more evaluations of the integrand.

APPENDIX C: COMPUTATIONAL FORMULAS FOR THE HO

The HO formulas obtained by combining Eqs. (26) and (A1)–(A3) look roughly similar to the MG formulas but are computable with less elaborate numerical methods. The KS orbitals are enumerated by the discrete index of the Hermite polynomials, making the η,η' sums of Eqs. (A1) and (A2) range from 0 to $N-1$. The number of occupied orbitals, N, is related to our input parameters $\bar{\lambda}$, $\bar{p}$ by

$$N=\left\lfloor \frac{1}{2\sqrt{2\bar{\lambda}\bar{p}^2}}+\frac{1}{2}\right\rfloor, \tag{C1}$$

where $\lfloor x\rfloor$ means the highest integer $\leqslant x$.

The speed of the calculations is increased by using an explicit expression for the Hermite polynomials in $z=0$. Furthermore, the function $g(r,r')$ is treated as in Appendix A, but without a lookup table, i.e., the function values are computed directly when needed.

All integrations in the HO model are performed by a straightforward implementation of adaptive Gaussian integration. The reason for not using the algorithm described in Appendix is that the HO model calculations were finished before the need for a parallelized integration algorithm for the MG case was discovered. This adds to the independence

of the two models, and makes the observation that computed values for the MG model approach values for the HO model an additional verification of our numerical methods.

APPENDIX D: CALCULATIONAL FORMULAS FOR THE GRADIENT AND LAPLACIAN

The density is calculated on a fully dimensionless form. For example, for the MG:

$$\bar{n}_m(\bar{z}) = \frac{n_m(\bar{z})}{n_u}. \tag{D1}$$

As a result, the dimensionless gradient s in Eq. (10), and Laplacian q in Eq. (11), take the forms

$$s = \frac{1}{2\bar{n}_m^{4/3}(\bar{z})}\left|\frac{d\bar{n}_m(\bar{z})}{d\bar{z}}\right|, \tag{D2}$$

$$q = \frac{1}{4\bar{n}_m^{5/3}(\bar{z})}\frac{d^2\bar{n}_m(\bar{z})}{d\bar{z}^2}. \tag{D3}$$

The quantities s and q can thus be easily computed by taking numerical derivatives of the routines that compute the density.

*Electronic address: rar@theophys.kth.se
†Electronic address: aematts@sandia.gov

[1] P. Hohenberg and W. Kohn, Phys. Rev. **136**, B864 (1964).
[2] W. Kohn and L. J. Sham, Phys. Rev. **140**, A1133 (1965).
[3] A correction procedure for such functionals has been proposed in Ref. 17 that takes care of the functional deficiency at surfaces. Similar, cruder procedures have successfully been applied to vacancy formation energies (Ref. 4) and work of adhesion (Ref. 5).
[4] K. Carling, G. Wahnström, T. R. Mattsson, A. E. Mattsson, N. Sandberg, and G. Grimvall, Phys. Rev. Lett. **85**, 3862 (2000); T. K. Mattsson and A. E. Mattsson (unpublished).
[5] A. E. Mattsson and D. R. Jennison, Surf. Sci. Lett. **520**, 611 (2002).
[6] W. Kohn and A. E. Mattsson, Phys. Rev. Lett. **81**, 3487 (1998).
[7] L. Vitos, B. Johansson, J. Kollár, and H. L. Skriver, Phys. Rev. B **62**, 10 046 (2000).
[8] J. P. Perdew and K. Schmidt, in *Density Functional Theory and Its Applications to Materials*, AIP Conf. Proc. No. 577, edited by V. Van Doren, C. Van Alsenoy, and P. Geerlings *et al.* (AIP, Melville, NY, 2001).
[9] N. A. Lima, M. F. Silva, L. N. Oliveira, and K. Capelle, cond-mat/0112428 (unpublished).
[10] M. Springborg, Chem. Phys. Lett. **308**, 83 (1999).
[11] J. Harris and R. O. Jones, J. Phys. F: Met. Phys. **4**, 1170 (1974); D. C. Langreth and J. P. Perdew, Solid State Commun. **17**, 1425 (1975); O. Gunnarsson and B. I. Lundquist, Phys. Rev. B **13**, 4274 (1976).
[12] L. Kleinman and S. Lee, Phys. Rev. B **37**, 4634 (1988).
[13] S. K. Ma and K. Brueckner, Phys. Rev. **165**, 18 (1968); K. H. Lau and W. Kohn, J. Phys. Chem. Solids **37**, 99 (1976); J. P. Perdew, D. C. Langreth, and V. Sahni, Phys. Rev. Lett. **38**, 1030 (1977).
[14] J. P. Perdew and Y. Wang, Phys. Rev. B **33**, 8800 (1986).
[15] J. P. Perdew, J. A. Chevary, S. H. Vosko, K. A. Jackson, M. R. Pederson, D. J. Singh, and C. Fiolhais, Phys. Rev. B **46**, 6671 (1992).
[16] D. M. Ceperley and B. J. Alder, Phys. Rev. Lett. **45**, 566 (1980).
[17] A. E. Mattsson and W. Kohn, J. Chem. Phys. **115**, 3441 (2001).
[18] V. Sahni, J. B. Krieger, and J. Gruenebaum, Phys. Rev. B **12**, 3503 (1975); V. Sahni, J. B. Krieger, and J. Gruenebaum, *ibid.* **15**, 1941 (1977); V. Sahni, C. Q. Ma, and J. S. Flamholz, *ibid.* **18**, 3931 (1978).
[19] S. Kurth, J. P. Perdew, and P. Blaha, Int. J. Quantum Chem. **75**, 889 (1999).
[20] L. M. Almeida, J. P. Perdew, C. Fiolhais, Phys. Rev. B **66**, 075115 (2002).
[21] J. P. Perdew, S. Kurth, A. Zupan, and P. Blaha, Phys. Rev. Lett. **82**, 2544 (1999).
[22] M. Nekovee, W. M. C. Foulkes, and R. J. Needs, Phys. Rev. Lett. **87**, 036401 (2001); M. Nekovee, W. M. C. Foulkes, A. J. Williamson, R. Rajagopal, and R. J. Needs, Adv. Quantum Chem. **31**, 189 (1999).
[23] J. C. Slater, Phys. Rev. **87**, 807 (1952).
[24] M. Abramowitz and I. A. Stegun, *Handbook of Mathematical Functions* (Dover, New York, 1964).
[25] N. W. Ashcroft and N. D. Mermin, *Solid State Physics* (Saunders College, Philadelphia, 1976).
[26] U. Gupta and A. K. Rajagopal, Phys. Rep. **87**, 259 (1982).
[27] P. S. Svendsen and U. von Barth, Phys. Rev. B **54**, 17 402 (1996).
[28] J. P. Perdew and Y. Wang, *Mathematics Applied to Science*, edited by J. A. Goldstein, S. I. Rosencrans, and G. A. Sod (Academic Press, Boston, 1988), pp. 187–209; L. Kleinman, Phys. Rev. B **10**, 2221 (1974).
[29] J. Tao, J. Chem. Phys. **115**, 3519 (2001).
[30] J. F. Hart, E. W. Cheney, C. L. Lawson, H. J. Maehly, C. K. Mesztenyi, J. R. Rice, H. G. Thacher, and C. Witzgall, *Computer Approximations* (Wiley, New York, 1968).
[31] W. H. Press, S. A. Teukolsky, W. T. Vetterling, and B. P. Flannery, *Numerical Recipes in C: The Art of Scientific Computing* (Cambridge University Press, Cambridge, England, 1992).
[32] R. B. Shirts, ACM Trans. Math. Softw. **19**, 377 (1993).
[33] R. Piessens, E. De Doncker-Kapenga, C. W. Uberhuber, and D. K. Kahaner, *QUADPACK, a Subroutine Package for Automatic Integration* (Springer, Berlin, 1983).